

Supporting Information

A graphene-like nanoribbon for efficient bifunctional electrocatalysts

Hongliang Peng¹†, Diancheng Duan^{1,2}†, Siyan Liu¹†, Jiayi Liu¹, Lixian Sun^{1}, Pengru Huang¹, Chunfeng Shao², Kexiang Zhang¹, Huanzhi Zhang¹, Xiaogang Xue¹, Fen Xu¹, Yongjin Zou¹, Yalin Liu³, Xinlong Tian^{3*} and Federico Rosei^{4*}*

- 1 Guangxi Key Laboratory of Information Material, School of Material Science and Engineering, Guilin University of Electronic Technology, Guilin, 54104, P. R. China
- 2 Key Laboratory of Fuel Cell Technology of Guangdong Province, School of Chemistry and Chemical Engineering, South China University of Technology, Guangzhou 510640, People's Republic of China
- 3 State Key Laboratory of Marine Resource Utilization in South China Sea, Hainan Provincial Key Lab of Fine Chemistry, School of Chemical Engineering and Technology, Hainan University, Haikou 570228, P. R. China
- 4 Institut National de la Recherche Scientifique, Centre Énergie, Matériaux et Télécommunications, 1650 Boul. Lionel Boulet, Varennes, J3X 1S2, Québec, Canada

† These authors contributed equally to this work

* Corresponding author. Tel: +86 18378310998 E -mail: sunlx@guet.edu.cn (Lixian Sun), tianxl@hainanu.edu.cn (Xinlong Tian), rosei@emt.inrs.ca (Federico Rosei)

Figures captions in Supporting Information

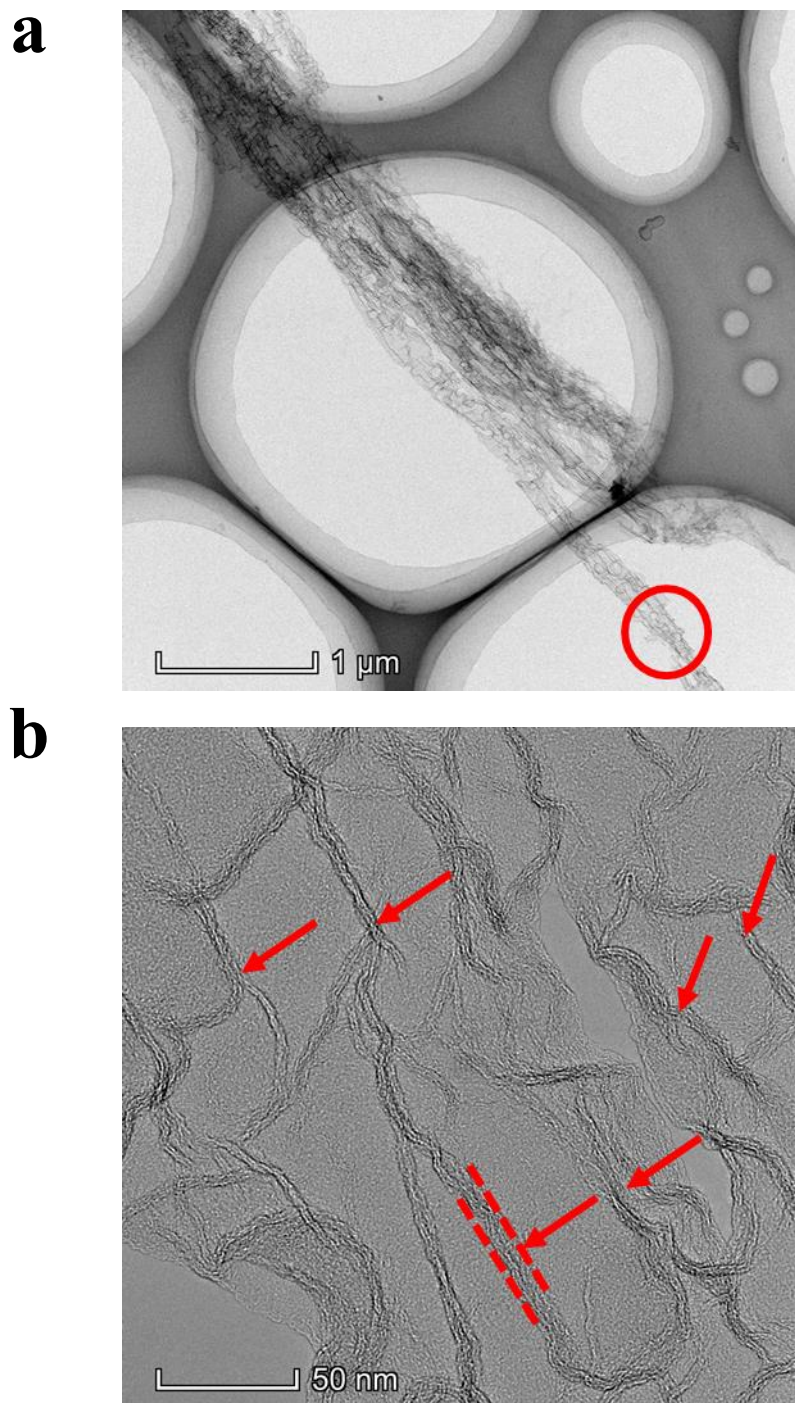


Fig. S1 (a, b) TEM images of C-MP-FeCo.

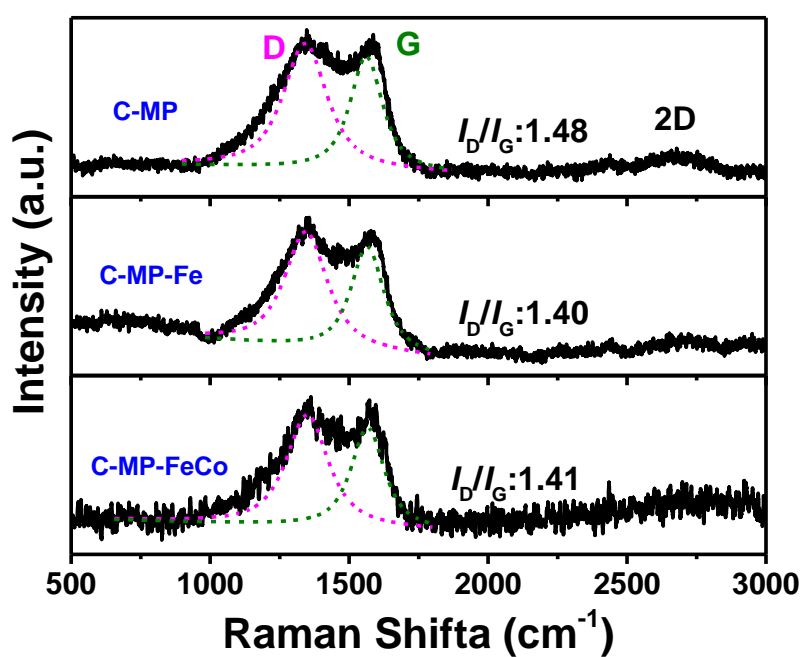


Fig. S2 Raman spectra of C-MP, C-MP-Fe and C-MP-FeCo.

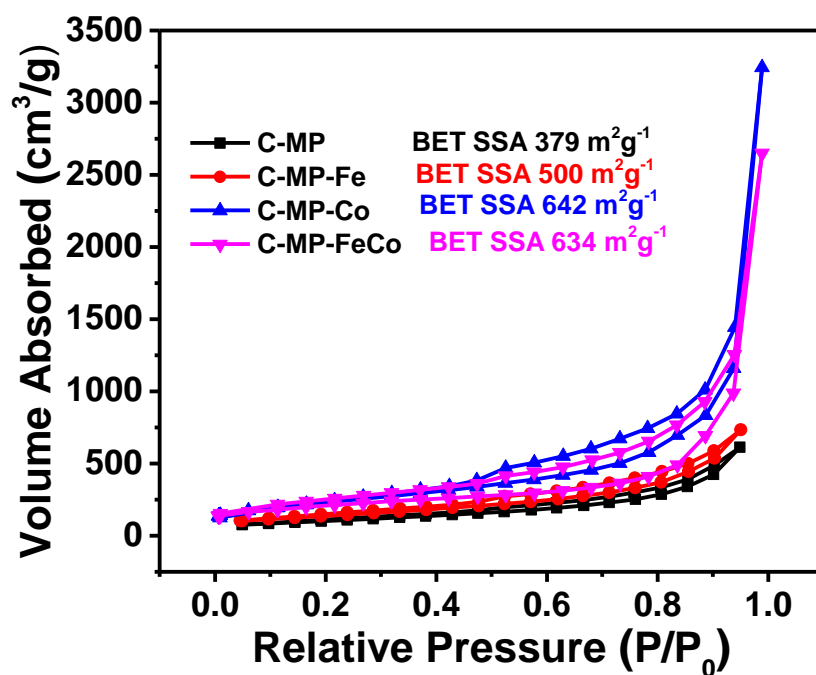


Fig. S3 N_2 adsorption-desorption isotherms of C-MP, C-MP-Fe, C-MP-Co and C-MP.

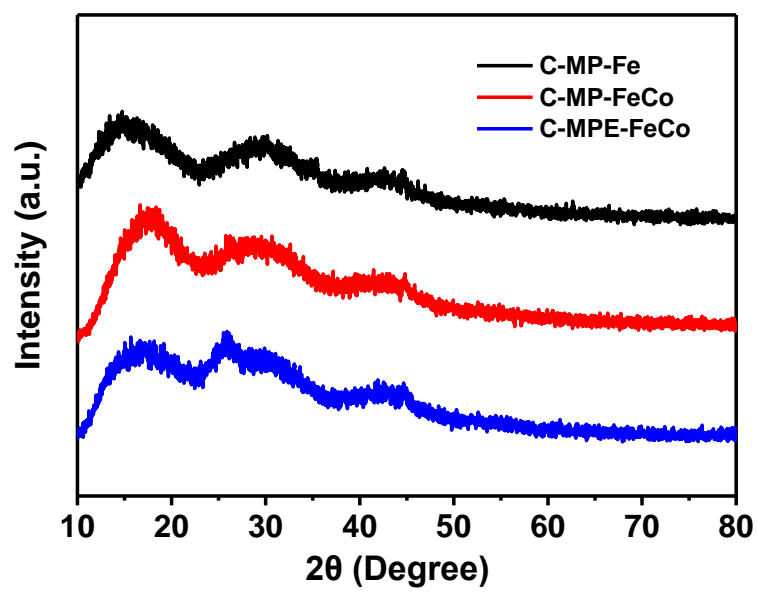


Fig. S4 XRD patterns of C-MP-Fe, C-MP-FeCo, and C-MPE-FeCo.

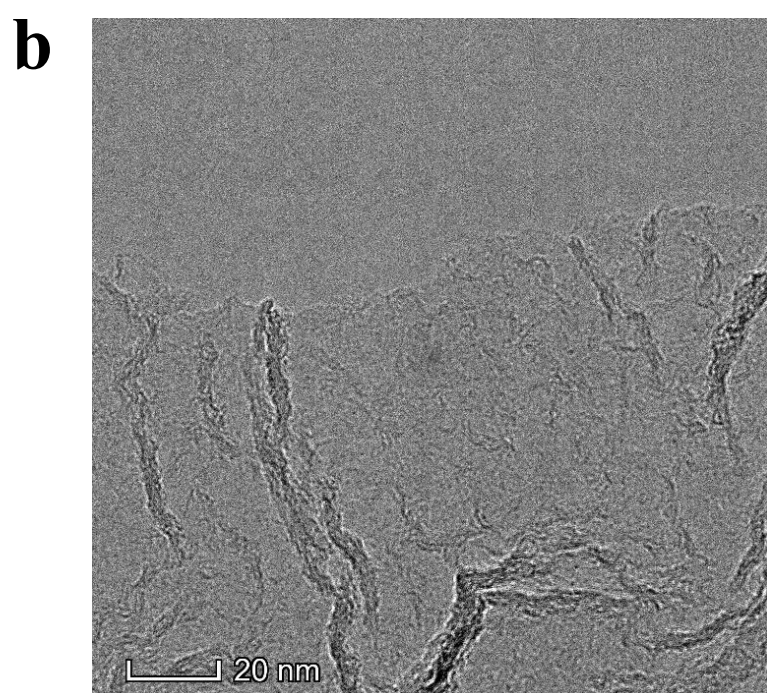
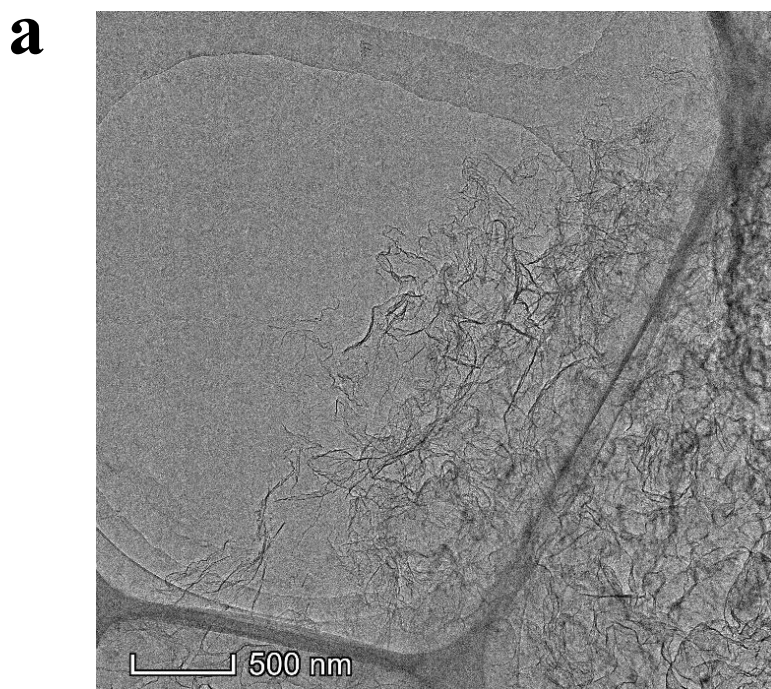
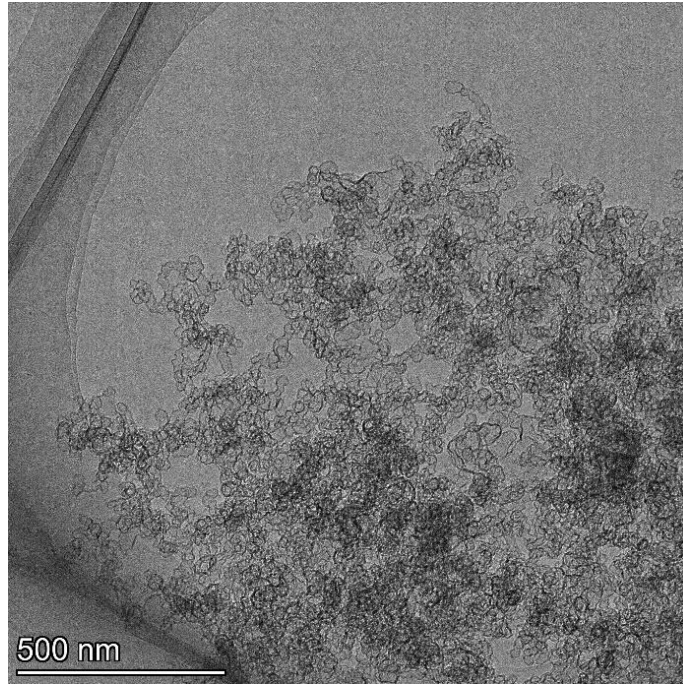


Fig. S5 (a, b) TEM images of C-MP-Co-2.

a



b

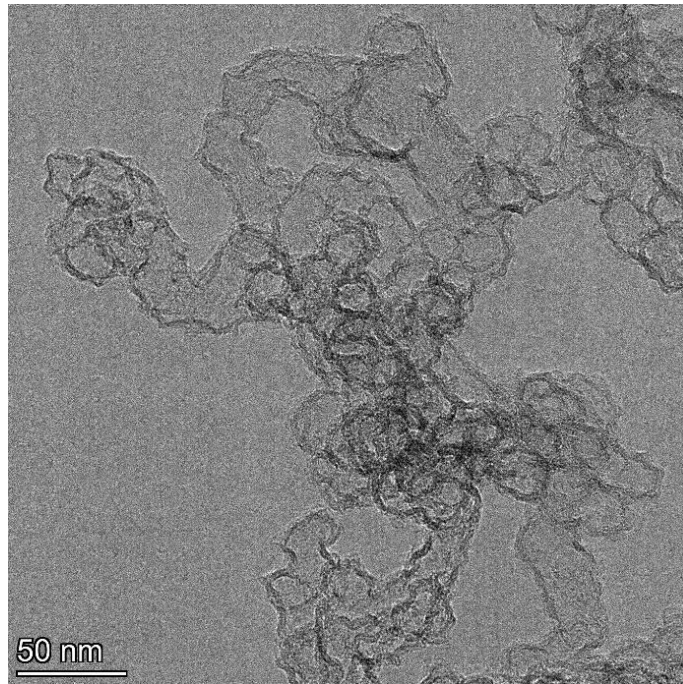
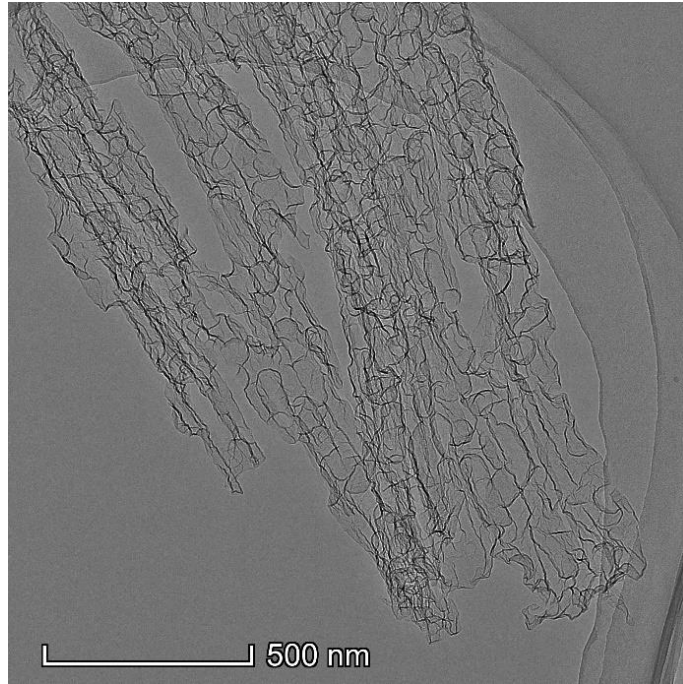


Fig. S6 (a, b) TEM images of C-MP-FeCo-28.

a



b

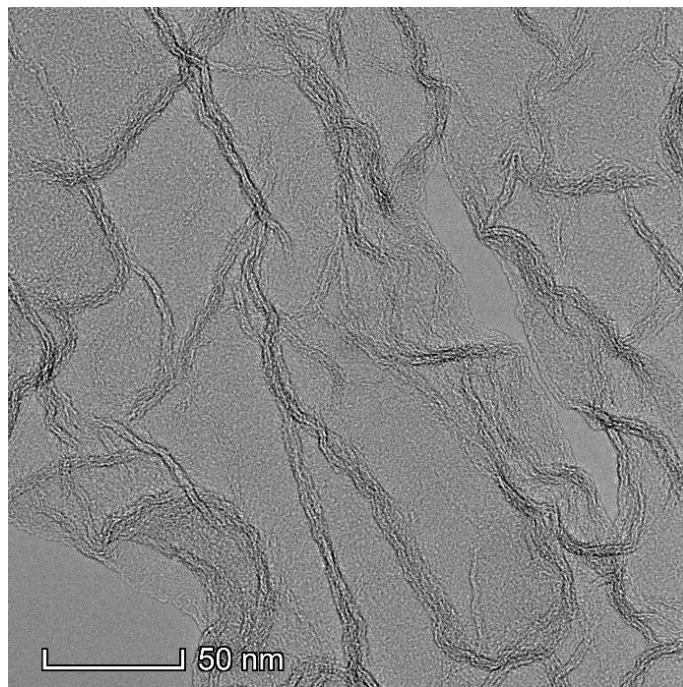
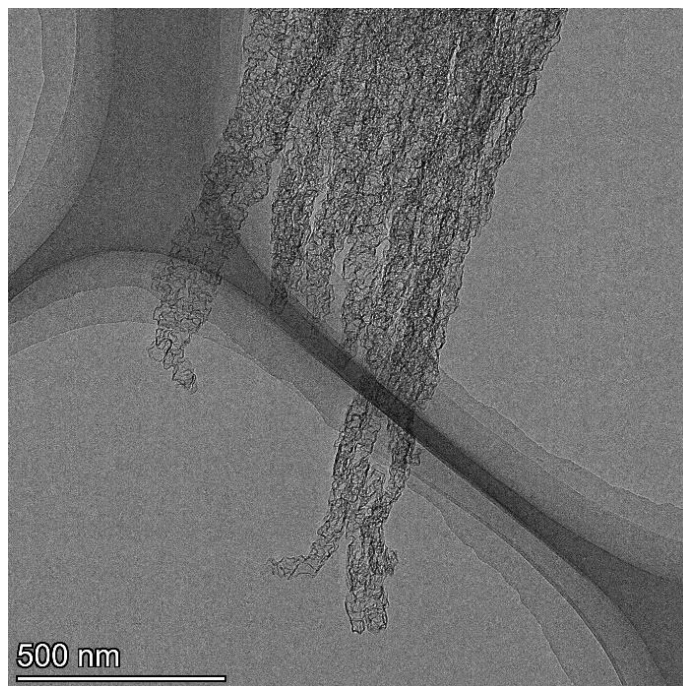


Fig. S7 (a, b) TEM images of C-MP-FeCo-11.

a



b

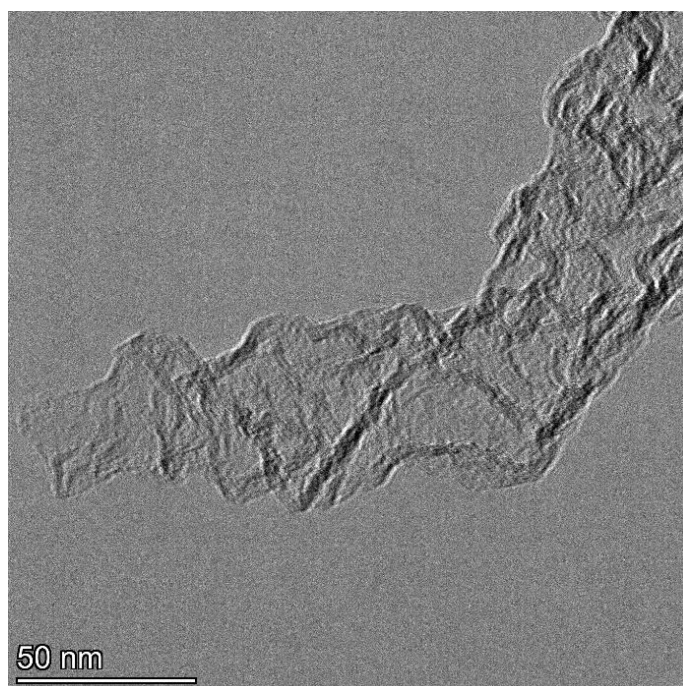


Fig. S8 (a, b) TEM images of C-MP-FeCo-82.

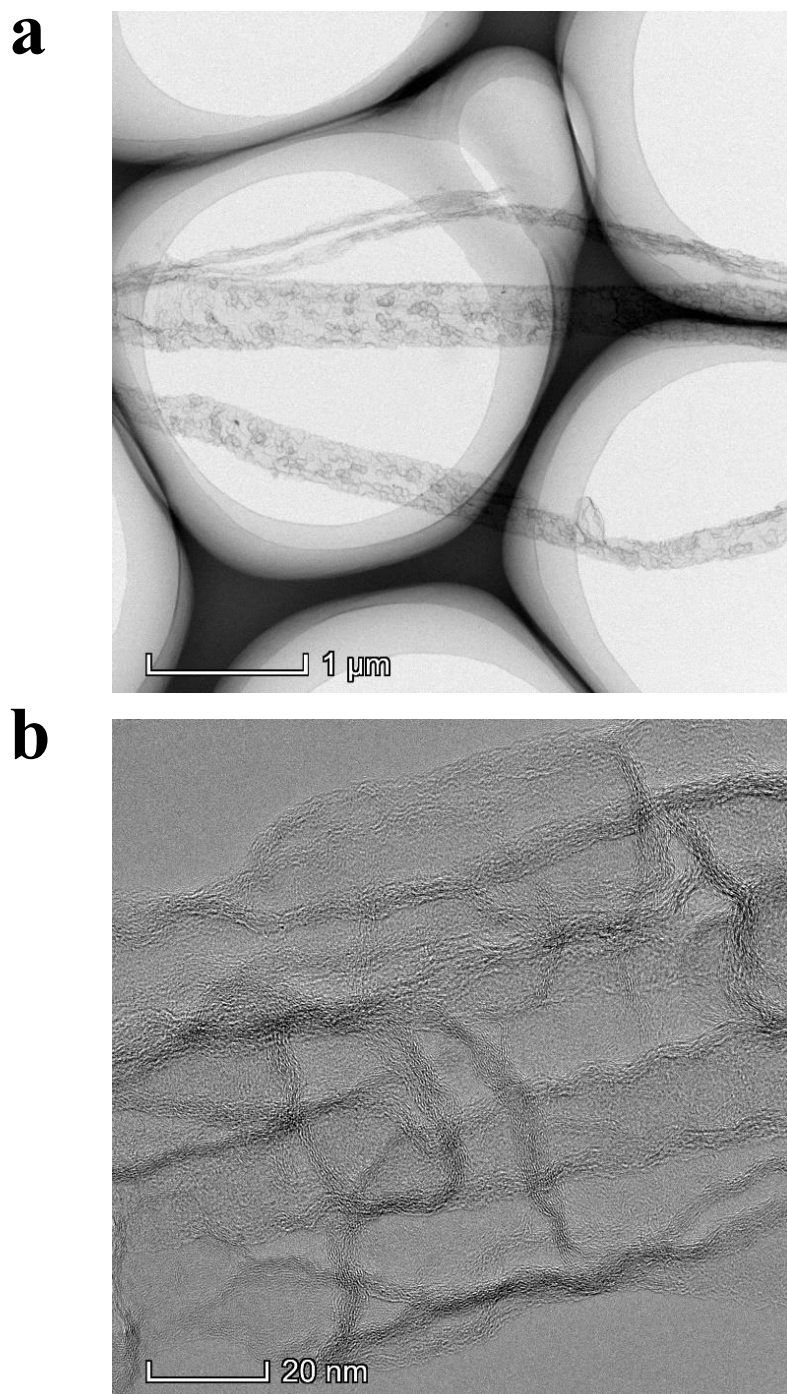


Fig. S9 (a, b) TEM images of C-MP-Fe-2.

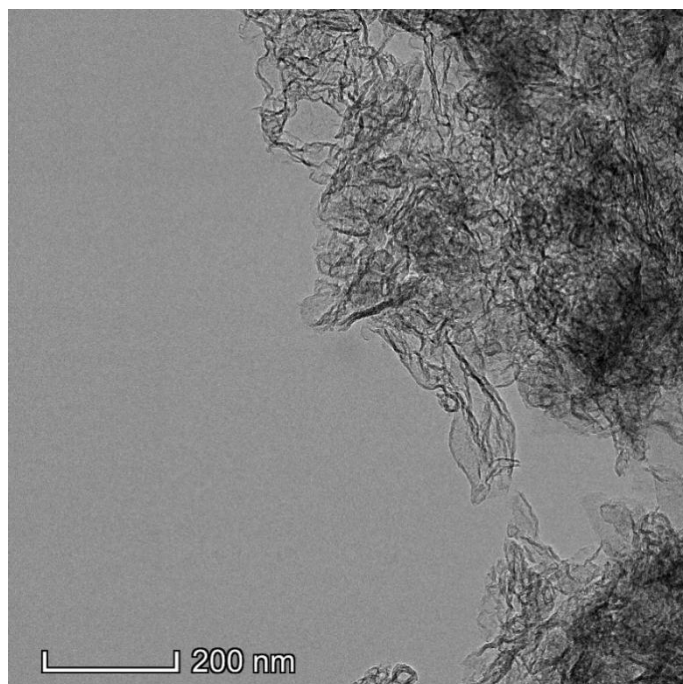
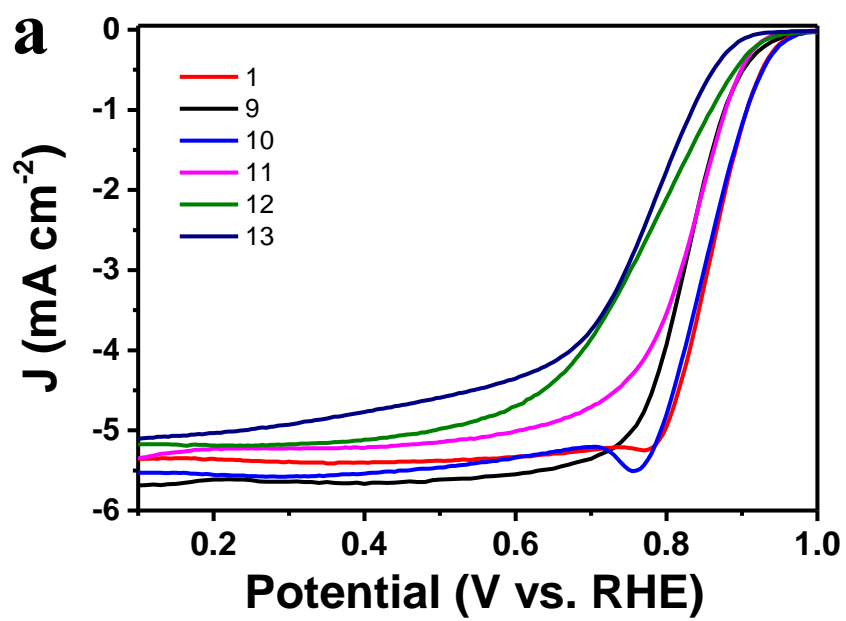


Fig. S10 TEM images of Fe- and Cu- codoped C-MP-FeCu catalysts.



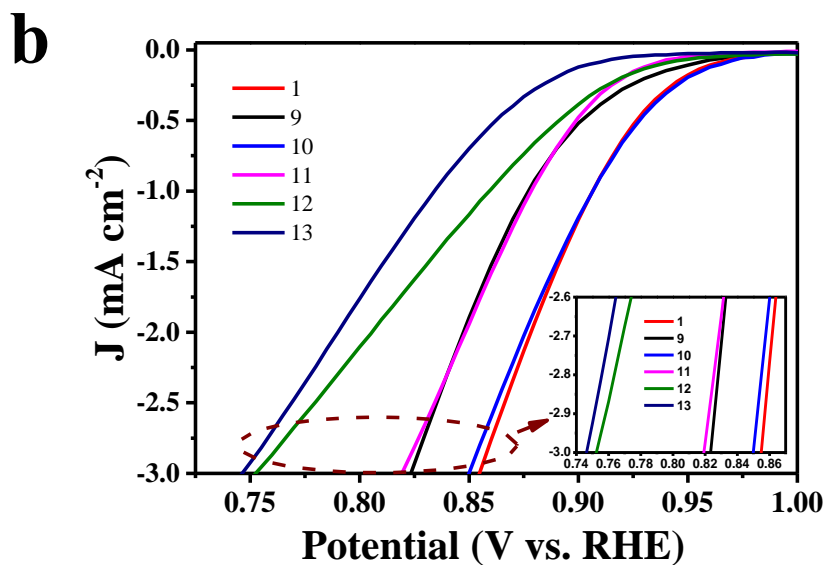


Fig. S11 (a, b) LSV curves of C-MP-Fe prepared at various pyrolysis temperatures: 1, 900 °C; 10, 950 °C; 11, 850 °C; 12, 800 °C; 13, 700 °C; and reference catalysts 9, Pt/C.

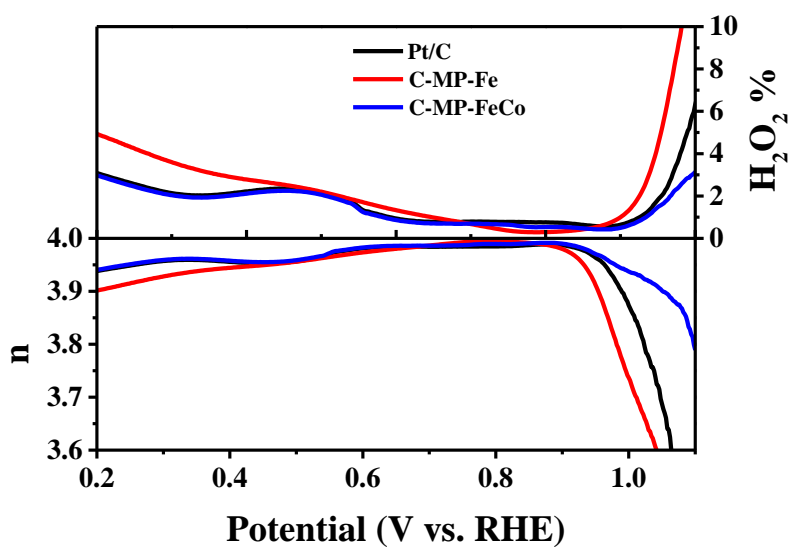


Fig. S12 H₂O₂ yield curves and the transferred electrons *n* for different catalysts measured at a scan rate of 5 mV s⁻¹.

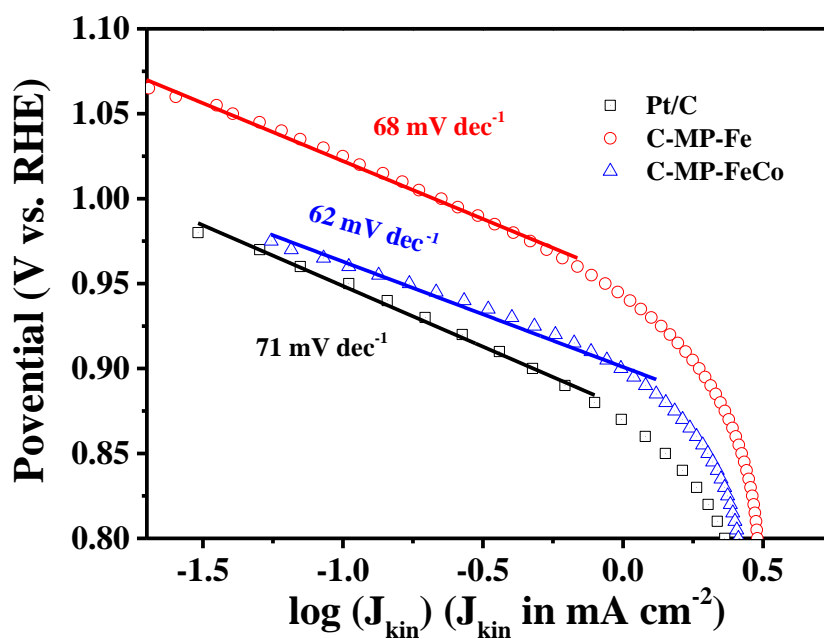


Fig. S13 ORR Tafel plots of different catalysts measured at a scan rate of 5 mV s^{-1} .

Tafel plots are obtained after the measured currents are corrected and calculated from the equation (1)¹.

$$J_{kin} = J \cdot J_{diff} / (J_{diff} - J) \quad (1)$$

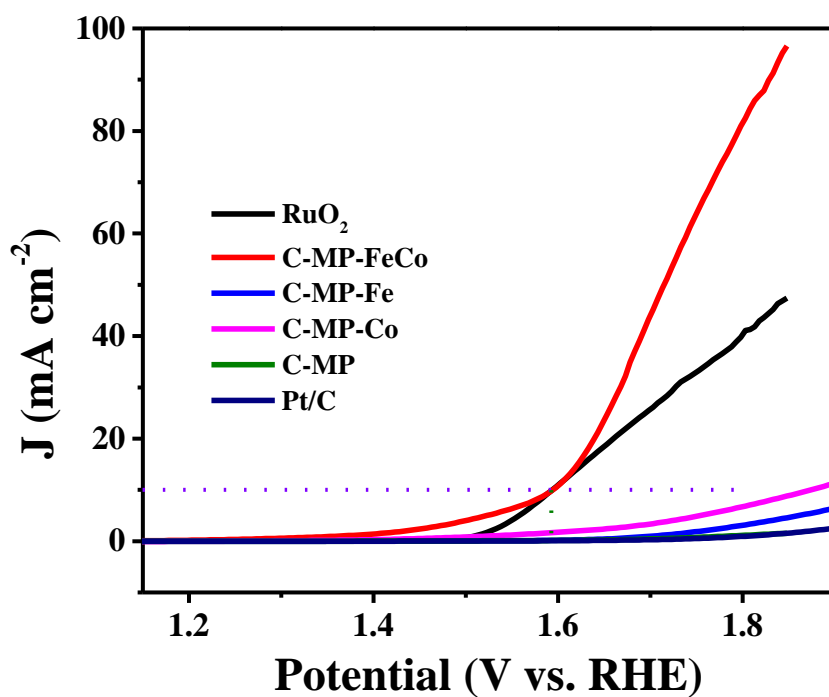


Fig. S14 OER polarization curves of different catalysts measured at a scan rate of 5 mV s^{-1} .

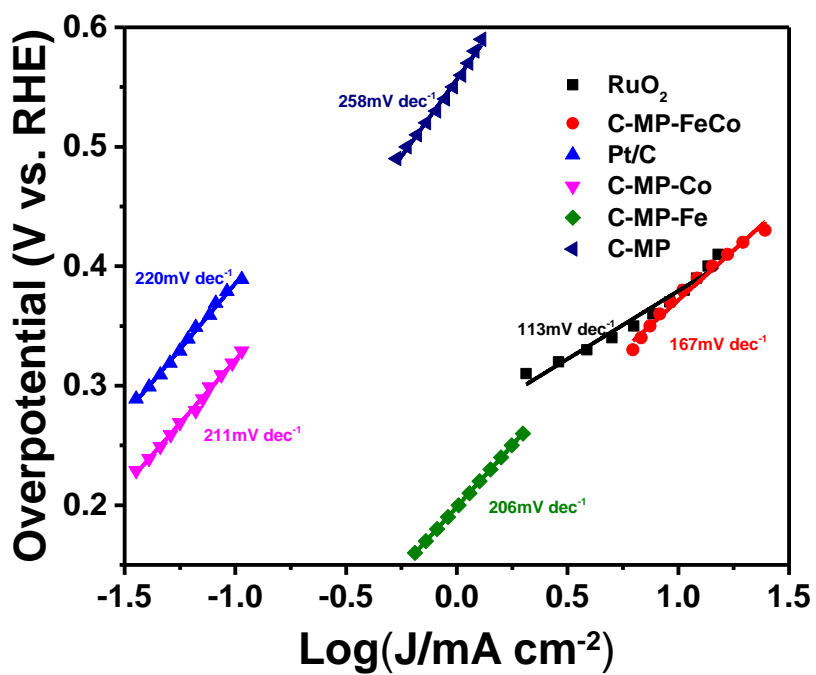


Fig. S15 The OER Tafel plots of different catalysts.

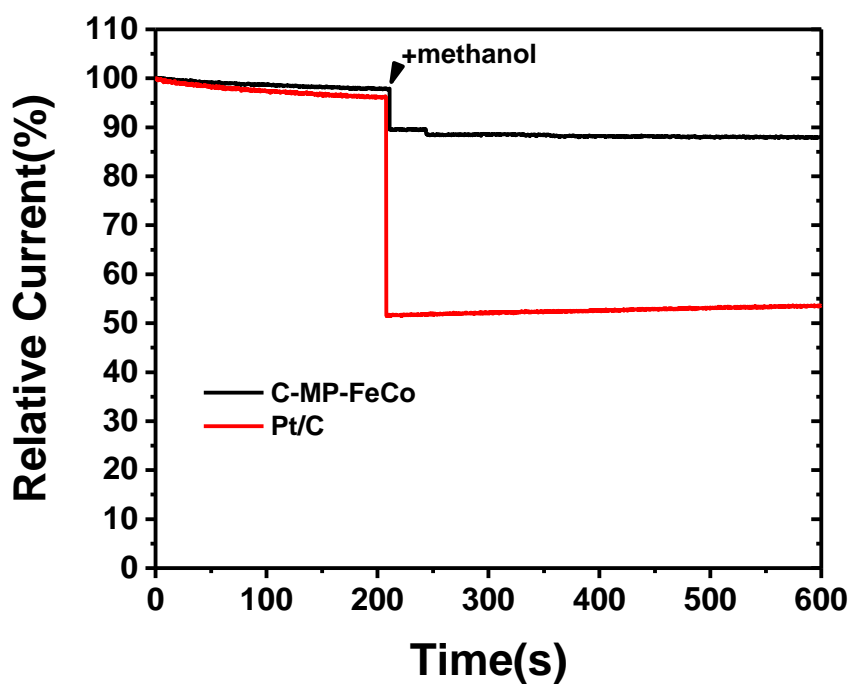
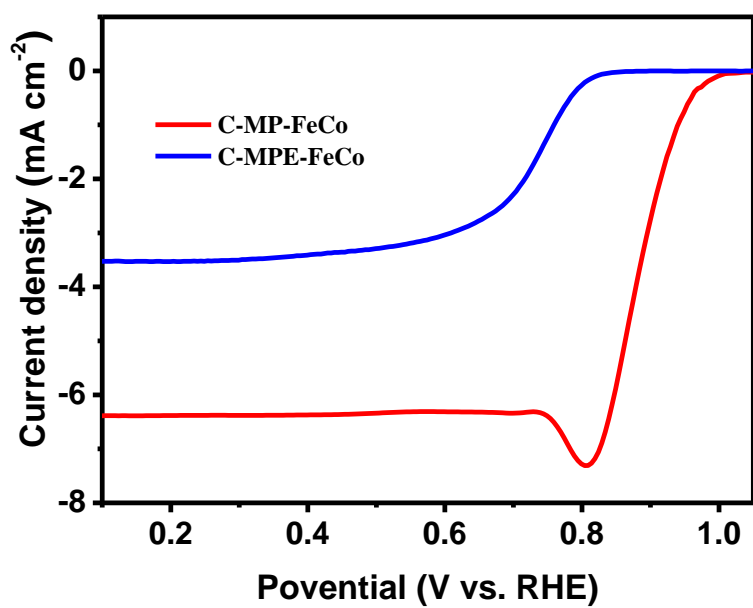


Fig. S16 Chronoamperometric responses of C-MP-FeCo and Pt/C after the addition of methanol.

a



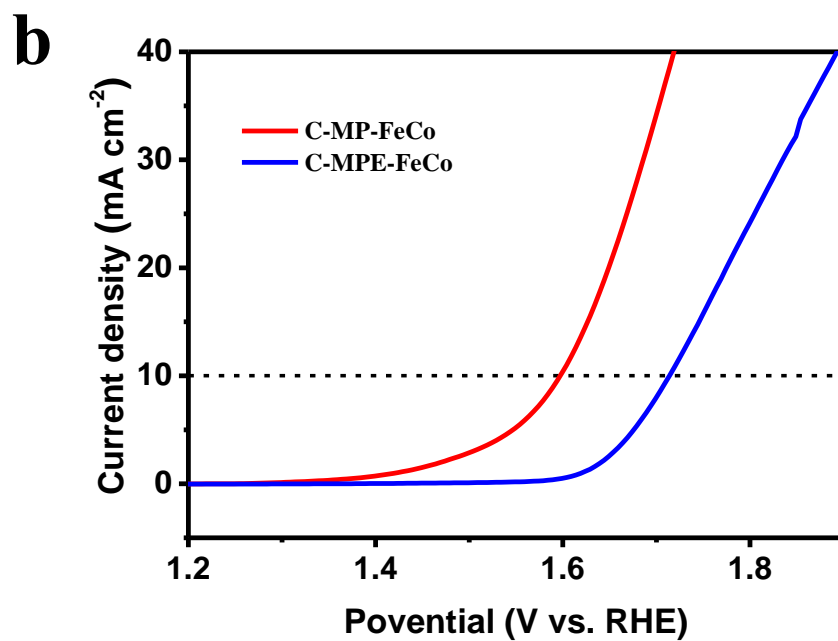
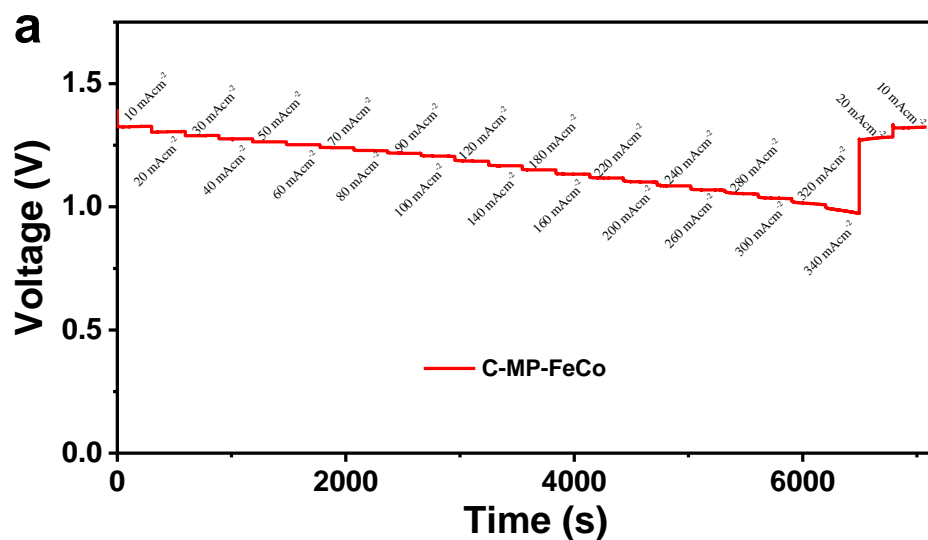


Fig. S17 (a) ORR and (b) OER polarization curves of C-MP-FeCo and C-MPE-FeCo measured at a scan rate of 5 mV s^{-1} .



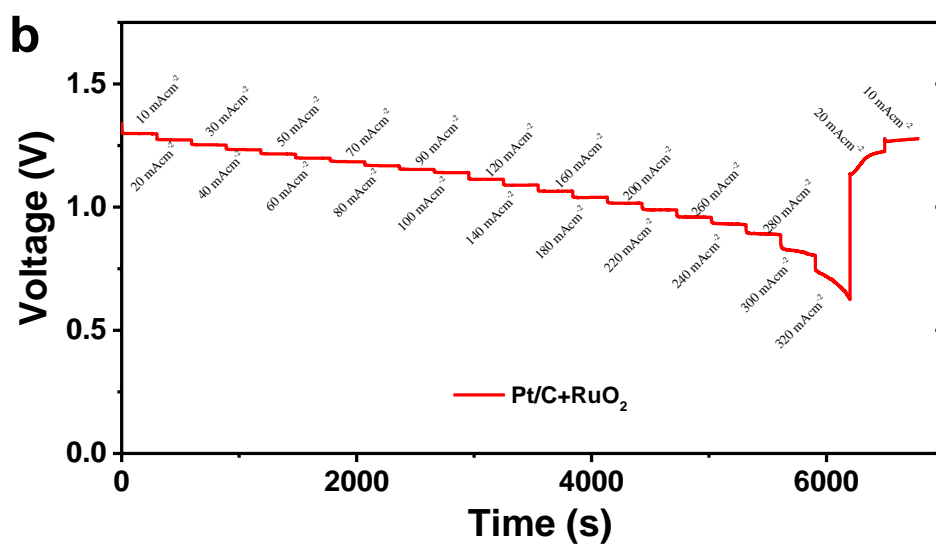


Fig. S18. Galvanostatic discharge curves of the Zn–air battery at different current densities: (a) C-MP-FeCo electrode (mass loading 5.5 mg cm⁻²); (b) Pt/C+RuO₂ electrode (mass loading 2.0 mg cm⁻²).

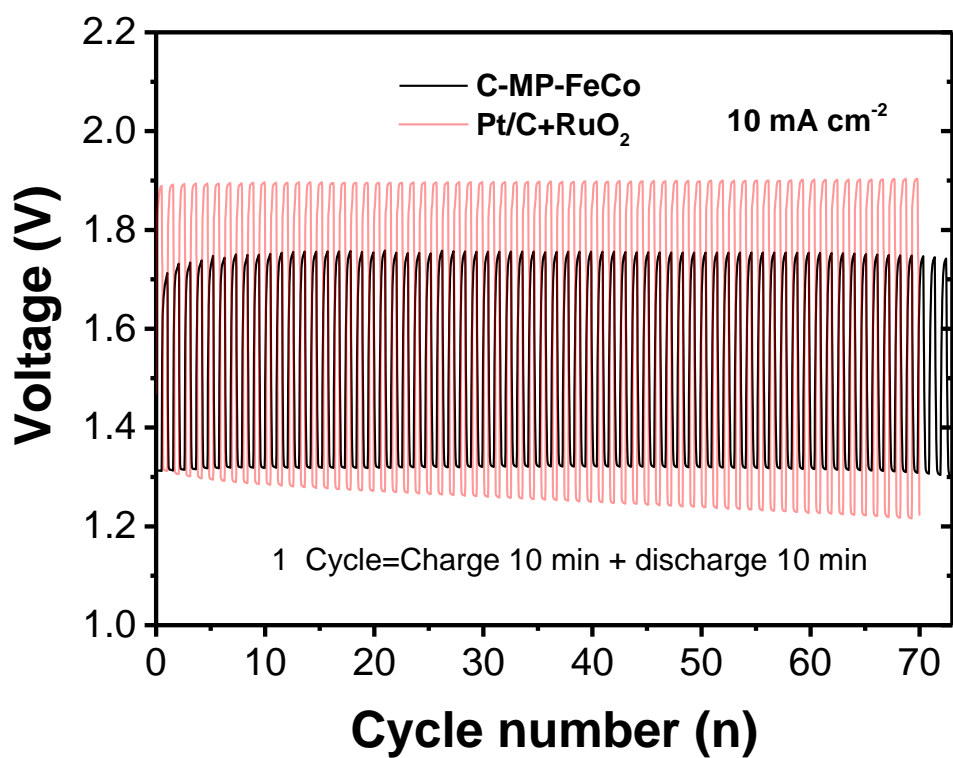


Fig. S19. Discharge and charge cycling of rechargeable Zn–air batteries based on Pt/C+RuO₂ and C-MP-FeCo electrode at the current density of 5 mA cm⁻².

Tables in Supporting Information

Table S1 The different preparation conditions of the sample 1 to sample 16.

| sample | T (°C) | Melamine (g) | PTFE (g) | PE (g) | 0.07 M FeCl ₃ (mL) | 0.07 M Co(CH ₃ COO) ₂ ·4H ₂ O (mL) |
|-----------------|---------|--------------|----------|--------|--------------------------------|---|
| 1(C-MP-Fe) | 900 | 5.0 | 7.5 | 0 | 2.0 | 0 |
| 2 | 900 | 5.0 | 7.5 | 0 | 1.5 | 0 |
| 3 | 900 | 5.0 | 7.5 | 0 | 8.0 | 0 |
| 4 | 900 | 5.0 | 7.5 | 0 | 4.0 | 0 |
| 5 | 900 | 5.0 | 7.5 | 0 | 3.0 | 0 |
| 6 | 900 | 5.0 | 7.5 | 0 | 1.0 | 0 |
| 7 | 900 | 5.0 | 7.5 | 0 | 0.5 | 0 |
| 8 (C-MP) | 900 | 5.0 | 7.5 | 0 | 0 | 0 |
| 9 (Pt/C) | / | / | / | 0 | / | / |
| 10 | 950 | 5.0 | 7.5 | 0 | 2.0 | 0 |
| 11 | 850 | 5.0 | 7.5 | 0 | 2.0 | 0 |
| 12 | 800 | 5.0 | 7.5 | 0 | 2.0 | 0 |
| 13 | 700 | 5.0 | 7.5 | 0 | 2.0 | 0 |
| 14(C-MP-FeCo) | 900 | 5.0 | 7.5 | 0 | 1.0 | 1.0 |
| 15(C-MP-Co) | 900 | 5.0 | 7.5 | 0 | 0 | 2.0 |
| 16 (C-MPE-FeCo) | 900 | 5.0 | 0 | 7.5 | 1.0 | 1.0 |

Table S2 The different preparation conditions of the different ratio of Fe/Co in C-

MP-FeCo sample

| sample | T (°C) | Melamine (g) | PTFE (g) | 0.07 M FeCl ₃ (mL) | 0.07 M Co(CH ₃ COO) ₂ ·4H ₂ O (mL) |
|--------------|---------|--------------|----------|--------------------------------|---|
| C-MP-Co-2 | 900 | 5.0 | 7.5 | 0 | 2.0 |
| C-MP-FeCo-28 | 900 | 5.0 | 7.5 | 2.0 | 8.0 |
| C-MP-FeCo-11 | 900 | 5.0 | 7.5 | 1.0 | 1.0 |
| C-MP-FeCo-82 | 900 | 5.0 | 7.5 | 8.0 | 2.0 |
| C-MP-Fe-2 | 900 | 5.0 | 7.5 | 2.0 | 0 |

Table S3. 2D-QSPR models for E_{onset} , $E_{1/2}$ and C_{Fe}

| Model | N | R | R^2 | Se | F |
|---|-----|--------|--------|--------|---------|
| $E_{\text{onset}}=-0.904(\pm 0.012)+0.144(\pm 0.030)\times C_{\text{Fe}}$ | 8 | 0.8930 | 0.7974 | 0.0165 | 23.6219 |
| $E_{1/2}=-0.755(\pm 0.016)+0.163(\pm 0.038)\times C_{\text{Fe}}$ | 8 | 0.8687 | 0.7546 | 0.0211 | 18.4524 |

Table S4. XPS surface element content (at%) and the ORR Kinetic Data for C-MP-Fe catalysts heat treatment at different temperatures.

| T (°C) | sample | Surface element content (at%) | | | | | potential (V) | |
|--------|--------|-------------------------------|------|------|-------|------|---------------|-----------|
| | | C | O | F | N | Fe | onset | half-wave |
| 900 | 1 | 90.01 | 1.24 | 0.63 | 7.67 | 0.45 | 0.98 | 0.855 |
| 950 | 10 | 90.43 | 1.27 | 0.45 | 7.48 | 0.38 | 0.99 | 0.85 |
| 850 | 11 | 67.79 | 2.52 | 0.57 | 28.3 | 0.82 | 0.965 | 0.82 |
| 800 | 12 | 77.77 | 2.58 | 0.63 | 18.28 | 0.75 | 0.97 | 0.755 |
| 700 | 13 | 67.49 | 1.36 | 0.68 | 29.97 | 0.49 | 0.93 | 0.745 |

Table S5. OER/OER performance comparisons of graphene(-like) nanoribbon, Nanosheets, CNT or graphitic carbon polyhedrons

| Sample | Morphology | Electrolyte | Potential(V) | | | Ref |
|---|--|------------------------------------|--------------|------------|------------------|-----|
| | | | $E_{1/2}^a$ | E_{10}^b | $E_{10}-E_{1/2}$ | |
| N-GRW | 3D graphene nanoribbon networks | 1.0 M KOH | 0.84 | 1.59 | 0.75 | 2 |
| DN-UGNR | Graphene Nanoribbons | 0.1 M KOH | 0.808 | 1.742 | 0.934 | 3 |
| Co ₃ O ₄ /N-csCNT-GNR | Carbon Nanotube/Graphene Nanoribbon | 0.1 M KOH | 0.81 | 1.89 | 0.78 | 4 |
| DN-CP@G | Graphene Nanosheets | 0.1 M KOH | 0.801 | 1.788 | 0.987 | 5 |
| Co ₃ Fe ₇ /NGNRs | graphene nanoribbon | 1.0 M KOH | 0.64 | 1.58 | 0.94 | 6 |
| N-HC@G-900 | holey carbon layer on a graphene sheet | 1.0 M KOH | 0.85 | 1.58 | 0.73 | 7 |
| MnO/Co/PGC | Porous graphitic carbon polyhedrons | 0.1 M KOH (ORR) 1.0 M KOH (OER) | 0.78 | 1.537 | 0.757 | 8 |
| NCN-1000-5 | ultrathin carbon nanosheets | 0.1 MKOH | 0.83 | 1.64 | 0.81 | 9 |
| Co-CoO/N-rGO | 3D Nanoporous | 0.1 MKOH | 0.78 | 1.62 | 0.84 | 10 |
| NOGB-800 | Graphene Nanorings | 0.1 MKOH (ORR) 1.0 MKOH (OER) | 0.84 | 1.65 | 0.81 | 11 |
| SHG | 2D graphitic sheet | 0.1 MKOH | 0.87 | 1.60 | 0.73 | 12 |
| P-3G | N-doped graphene | 0.1 MKOH | 0.82 | 1.54 | 0.72 | 13 |
| FeCo-DHO/NCNTs | Fe,Co-doped NCNTs | 1.0 M KOH | 0.86 | 1.55 | 0.69 | 14 |

| | | | | | | |
|---------------------------------|--|----------|-------|-------|------|--------------|
| FeCo/Co ₂ P@NP CF | FeCo/Co ₂ P Hybrid Nanoparticles | 0.1 MKOH | 0.79 | 1.56 | 0.77 | 15 |
| C-MP-FeCo | graphene-lik nanoribbon | 0.1 MKOH | 0.895 | 1.595 | 0.70 | This work |

a: Half-wave potential of ORR.

b: Potential at 10 mA cm⁻² of OER

References

1. M. Jahan, Z. L. Liu and K. P. Loh, *Adv. Funct. Mater.*, 2013, **23**, 5363-5372.
2. H. B. Yang, J. W. Miao, S. F. Hung, J. Z. Chen, H. B. Tao, X. Z. Wang, L. P. Zhang, R. Chen, J. J. Gao, H. M. Chen, L. M. Dai and B. Liu, *Sci. Adv.*, 2016, **2**, 11.
3. J. Zhang, Y. Sun, J. Zhu, Z. Gao, S. Li, S. Mu and Y. Huang, *Adv. Sci.*, 2018, **5**, 1801375.
4. X. Y. Lu, H. M. Chan, C. L. Sun, C. M. Tseng and C. Zhao, *J. Mater. Chem. A*, 2015, **3**, 13371-13376.
5. C. Hang, J. Zhang, J. Zhu, W. Li, Z. Kou and Y. Huang, *Adv. Energy Mater.*, 2018, **8**, 9.
6. J. Joy, S. Rajappa, V. K. Pillai and S. Alwarappan, *Nanotechnology*, 2018, **29**, 8.
7. J. Sun, S. E. Lowe, L. Zhang, Y. Wang, K. Pang, Y. Wang, Y. Zhong, P. Liu, K. Zhao, Z. Tang and H. Zhao, *Angew. Chem. Int. Edit.*, 2018, **57**, 16511-16515.
8. X. F. Lu, Y. Chen, S. Wang, S. Gao and X. W. D. Lou, *Adv. Mater.*, 2019, **31**, 8.
9. H. Jiang, J. X. Gu, X. S. Zheng, M. Liu, X. Q. Qiu, L. B. Wang, W. Z. Li, Z. F. Chen, X. B. Ji and J. Li, *Energ. environ. Sci.*, 2019, **12**, 322-333.
10. X. Liu, W. Liu, M. Ko, M. Park, M. G. Kim, P. Oh, S. Chae, S. Park, A. Casimir, G. Wu and J. Cho, *Adv. Funct. Mater.*, 2015, **25**, 5799-5808.
11. Q. Hu, G. M. Li, G. D. Li, X. F. Liu, B. Zhu, X. Y. Chai, Q. L. Zhang, J. Liu and C. He, *Adv. Energy Mater.*, 2019, **9**, 9.
12. C. G. Hu and L. M. Dai, *Adv. Mater.*, 2017, **29**, 9.
13. Y. F. Bu, H. Jang, O. Gwon, S. H. Kim, S. H. Joo, G. Nam, S. Kim, Y. Qin, Q. Zhong, S. K. Kwak, J. Cho and G. Kim, *J. Mater. Chem. A*, 2019, **7**, 2048-2054.
14. M. J. Wu, Q. L. Wei, G. X. Zhang, J. L. Qiao, M. X. Wu, J. H. Zhang, Q. J. Gong and S. H. Sun, *Adv. Energy Mater.*, 2018, **8**, 10.
15. Q. Shi, Q. Liu, Y. Ma, Z. Fang, Z. Liang, G. Shao, B. Tang, W. Yang, L. Qin and X. Fang, *Adv. Energy Mater.*, 2020, **10**, 1903854.